



TURBULENCE-GENERATED PROTON-SCALE STRUCTURES IN THE TERRESTRIAL MAGNETOSHEATH

ZOLTÁN VÖRÖS^{1,2}, EMILIYA YORDANOVA³, MARIUS M. ECHIM^{4,5}, GIUSEPPE CONSOLINI⁶, AND YASUHITO NARITA¹¹Space Research Institute, Austrian Academy of Sciences, Graz, Austria; zoltan.voeroes@oeaw.ac.at²Department of Geophysics and Space Sciences, Eötvös University, Budapest, Hungary³Swedish Institute of Space Physics, Uppsala, Sweden⁴Belgian Institute for Space Aeronomy, Bruxelles, Belgium⁵Institute for Space Sciences, Măgurele, Romania⁶INAF-Istituto di Astrofisica e Planetologia Spaziali, Roma, Italy

Received 2016 January 25; accepted 2016 February 12; published 2016 March 1

ABSTRACT

Recent results of numerical magnetohydrodynamic simulations suggest that in collisionless space plasmas, turbulence can spontaneously generate thin current sheets. These coherent structures can partially explain the intermittency and the non-homogenous distribution of localized plasma heating in turbulence. In this Letter, *Cluster* multi-point observations are used to investigate the distribution of magnetic field discontinuities and the associated small-scale current sheets in the terrestrial magnetosheath downstream of a quasi-parallel bow shock. It is shown experimentally, for the first time, that the strongest turbulence-generated current sheets occupy the long tails of probability distribution functions associated with extremal values of magnetic field partial derivatives. During the analyzed one-hour time interval, about a hundred strong discontinuities, possibly proton-scale current sheets, were observed.

Key words: magnetic fields – magnetic reconnection – plasmas – turbulence

1. INTRODUCTION

Downstream of the terrestrial bow shock (BS), the supersonic and super-Alfvénic solar wind flow slows down and gets compressed and heated. The solar wind is diverted by the strong geomagnetic field at the magnetopause (MP). The magnetosheath (MS) is the region between the BS and the MP, where the field and plasma fluctuations are rather strong. Numerical simulations (Karimabadi et al. 2014; Omidi et al. 2014) demonstrate the complexity of this region—being populated by various interacting multi-scale structures, such as filaments, vortices, current sheets, plasma jets, and flows. In situ measurements from different missions also revealed the existence of nonlinear structures in upstream and downstream BS regions, for example, shocklets (Hoppe et al. 1981), short-duration large-amplitude magnetic structures (Lucek et al. 2004), and hot-flow anomalies (Facsó et al. 2009) embedded in the highly turbulent MS. Some of these nonlinear structures are also associated with enhanced levels of wave and fluctuation activity (Kovács et al. 2014). The fluctuations and structures are more pronounced in the quasi-parallel BS configuration when the angle between the interplanetary magnetic field and the nominal BS normal is smaller than 45° . In such a case, the upstream (solar wind, foreshock) and downstream MS regions are magnetically connected and the resulting turbulence becomes increasingly intermittent away from the BS (Yordanova et al. 2008).

In turbulent space plasmas, thin magnetic structures, current sheets, and reconnection can be generated spontaneously through complex interactions (Chang et al. 2004; Servidio et al. 2009; Matthaeus et al. 2015). Furthermore, recent studies on the statistics of velocity gradient tensor invariants revealed that approaching the non-MHD scales, vortex stretching may play a relevant role in generating small-scale dissipative structures (Consolini et al. 2015). These structures observed as discontinuities in the solar wind (Greco et al. 2009) are associated with local dissipation/heating (Osman

et al. 2012, 2014) and introduce intermittency to plasma turbulence. The occurrence frequency of discontinuities in the solar wind agrees rather well with the statistics of turbulence-generated current sheets in numerical simulations (Greco et al. 2008, 2009; Servidio et al. 2011). *Cluster* observations in MS downstream quasi-parallel BS also confirmed the occurrence of reconnecting thin current sheets (Retinò et al. 2007; Sundkvist et al. 2007) and the current sheet associated electron heating (Chasapis et al. 2015b).

Numerical simulations have shown that the strongest discontinuities and current sheets generated by turbulence populate the tails of non-Gaussian probability distribution functions (PDFs) of the normalized current density (Greco et al. 2009; Matthaeus et al. 2015). However, this has not been shown directly from the data. Although it is tempting to assume that the fat tails of the PDFs are completely determined by turbulence-generated strong current sheets, one should not forget that there might exist other intermittent structures of different origin. As a matter of fact, the high Reynolds number simulations of MHD turbulence (Greco et al. 2009; Servidio et al. 2011) cannot reproduce the rich ensemble of intermittent nonlinear structures mentioned above. In this Letter, using *Cluster* data in the MS downstream of quasi-parallel BSs, we show that the strongest observed current sheets de facto occupy the tails of histograms. We also estimate the occurrence frequency of the strongest current sheets along the trajectory of the *Cluster* spacecraft. The paper is organized as follows. Section 2 explains the data and instrumentation and Section 3 introduces the structure detection tools. Section 4 demonstrates how the structure detection tools work for a thin current sheet. In Section 5, discontinuity and current sheet statistics is presented. Section 6 contains the summary and conclusions.

2. DATA AND INSTRUMENTATION

In this Letter we consider the data interval between 9.6 and 10.6 UT (decimal hours) on 2002 March 27 when the *Cluster*

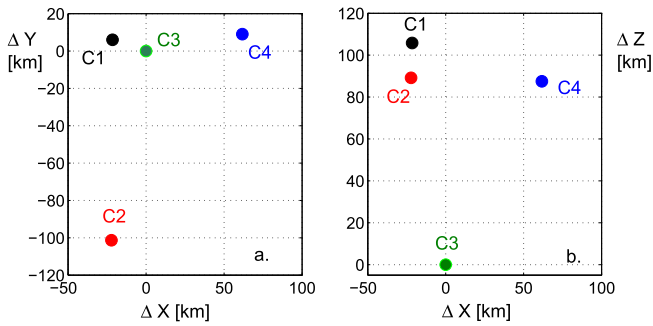


Figure 1. Relative positions of the *Cluster* spacecraft. (a) ΔX vs. ΔY ; (b) ΔX vs. ΔZ .

spacecraft probed the magnetosheath downstream of a quasi-parallel BS. OMNI 1 minute data have been used to obtain the model BS (Farris & Russell 1994) and magnetopause (Shue et al. 1998) boundaries as well as the normal vector to the BS. The *Cluster* fleet was initially at the GSE coordinate system position (10, -8.2, -8) R_E , moving $\sim 1R_E$ toward the magnetopause in a nearly perfect tetrahedron configuration with inter-probe separations of about 100 km. The relative positions of the spacecraft are shown in Figure 1. The upstream plasma and field conditions in the solar wind were quasi-stationary with average parameters—magnetic field ~ 3.4 nT, velocity ~ 446 km s^{-1} , and density ~ 3 cm^{-3} .

During the selected interval, the magnetic field measurements were available from the FGM instrument (Balogh et al. 1997) with sampling frequency $f_s = 67$ Hz, and from the STAFF instrument (Cornilleau-Wehrlin et al. 1997) with $f_s = 450$ Hz. Using a finite impulse response filter at ~ 1 Hz, the magnetic data from both instruments were merged into one time series with extended frequency coverage up to 450 Hz in burst mode. The electric field data were available from the EFW instrument (Gustafsson et al. 1997).

3. STRUCTURE DETECTION TOOLS

Current sheets associated with large-scale boundaries such as the magnetopause or the magnetotail current sheet can be easily identified. Even if the boundaries are moving or the structures are flapping, the same current sheet can be observed multiple times. On the other hand, turbulence-generated boundaries and the associated current sheets are small-scale and transient in the spacecraft frame. Their identification requires special methods. To detect discontinuities and current sheets in the magnetosheath, three types of parameters will be estimated from *Cluster* spacecraft pairs ($C_i - C_j$, $i, j = 1, 2, 3, 4$) in time t : (1) the Partial Variance of Increments (PVI $_{ij}(t)$); (2) the angle between magnetic field vectors $\theta_{ij}(t)$; and (3) the magnetic field derivatives $\partial_{ij}(t)$.

The method using PVIs was first introduced to identify discontinuities within the intermittent solar wind turbulence from a single point measurement. The results have also been supported by numerical simulations (Greco et al. 2009). The PVIs here are calculated on the basis of the normalized variance of the absolute value of magnetic field spatial increments between two spacecraft $\Delta \mathbf{B}_{ij}(t) = \mathbf{B}_i(t) - \mathbf{B}_j(t)$:

$$PVI_{ij}(t) = \sqrt{\frac{|\Delta \mathbf{B}_{ij}(t)|^2}{\langle |\Delta \mathbf{B}_{ij}|^2 \rangle}}, \quad (1)$$

where the average $\langle \cdot \rangle$ is taken over the whole interval. The mean $PVI_m(t) = \sum_{ij} PVI_{ij}(t)/6$ is also calculated. In contrary to the standard one-directional PVI (Greco et al. 2008), PVI m comprises information on increments along all $C_i - C_j$ pairs in the *Cluster* tetrahedron. In recent 3D simulations of MHD turbulence, a similar multi-directional PVI was used, arguably providing an unbiased information about the spatial structure of discontinuities (Zhang et al. 2015).

The rotation of the magnetic field vector between spacecraft pairs is estimated through

$$\theta_{ij}(t) = \cos^{-1} \frac{\mathbf{B}_i(t) \cdot \mathbf{B}_j(t)}{|\mathbf{B}_i(t)| \cdot |\mathbf{B}_j(t)|}. \quad (2)$$

The partial derivatives of the magnetic field are obtained from

$$\partial_{ij}(t) \equiv \frac{\Delta \mathbf{B}_{ij}(t)}{\Delta \mathbf{r}_{ij}(t)} \quad (3)$$

where $\Delta \mathbf{r}_{ij}(t)$ is the spatial separation between C_i , C_j pairs and ∂_{ij} stands for the partial derivatives $\partial B_x / \partial X$, $\partial B_x / \partial Y$, $\partial B_x / \partial Z$, etc. These form the orthogonal components of $(\nabla \times \mathbf{B})_{xyz}$ and $(\nabla \cdot \mathbf{B})_{xyz}$. For supposedly time-independent short events with roughly constant $(\nabla \times \mathbf{B})_{xyz}$ and for linearly changing magnitudes of magnetic components over the tetrahedron, the current density $\mathbf{j} = (\nabla \times \mathbf{B}) / \mu_0$ (μ_0 is the magnetic constant) can be calculated.

It has already been shown that the parameters PVI and θ are correlated. Discontinuities with high values of PVI are associated with large magnetic rotations $\theta > 90^\circ$ (Chasapis et al. 2015b). The joint occurrence of strong magnetic shear and high PVI indicates that the corresponding discontinuity is a current sheet. More about structure detection tools in turbulence can be found in Chasapis (2015a). For the studied interval, the correlations are demonstrated in Figure 2. The left panels 2(a)–(d) show the magnetic field intensity for C1, the PVI magnitude for the spacecraft pair C1–C4, the magnetic field rotation angle for the same pair of probes, and the partial derivatives for the B_z components of the magnetic field. The parameters from the other spacecraft or spacecraft pairs look similar (not shown). The right panels 2(e)–(h) show the PDFs corresponding to the time series on the left. The maxima of the PDFs are normalized to one. Gaussians with the same standard deviations are inserted as well. Although the PDF of $B(C1)$ is the closest to the Gaussian distribution, there are significant deviations from it near the peak value. It indicates that various physical processes with different magnetic PDFs can form the summary histogram within the analyzed interval. The large deviations from the Gaussians for the other parameters are evident near the maxima and at the tails of PDFs. Since the strongest discontinuities or (reconnecting) current sheets are expected to form the tail of PDFs (Greco et al. 2009), we are interested in correlations between the extremal values of PVI $_{ij}$, θ_{ij} and ∂_{ij} . The green boxes in panels 2(a)–(d) show a few sub-intervals of the data when the threshold $PVI(C1-C4) = 4$ selects intervals of large deviations of θ_{ij} and ∂_{ij} as well.

4. AN EXAMPLE CURRENT SHEET

Figure 3 shows a crossing of a thin proton-scale (~ 0.5 s) current sheet by the *Cluster* fleet, for which Chasapis et al. (2015b) found electron heating signatures. For this event the

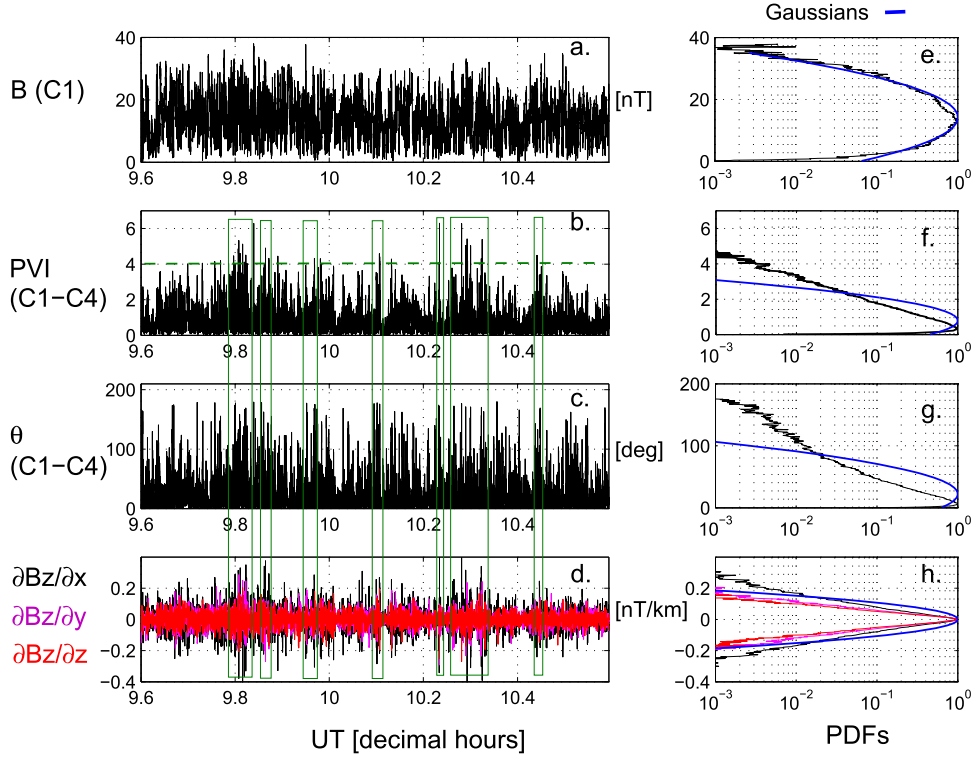


Figure 2. Left panels (a)–(d): magnetic field intensity for C1; PVI magnitude for C1–C4 with threshold 4 (dashed green line); magnetic field rotation angle for C1–C4; and partial derivatives of the magnetic field B_z component. The boxes outlined in green show examples of detected discontinuities above the given threshold PVI = 4. Right panels (e)–(h): PDFs (histograms) corresponding to the data on the left. Gaussian distributions are shown in blue.

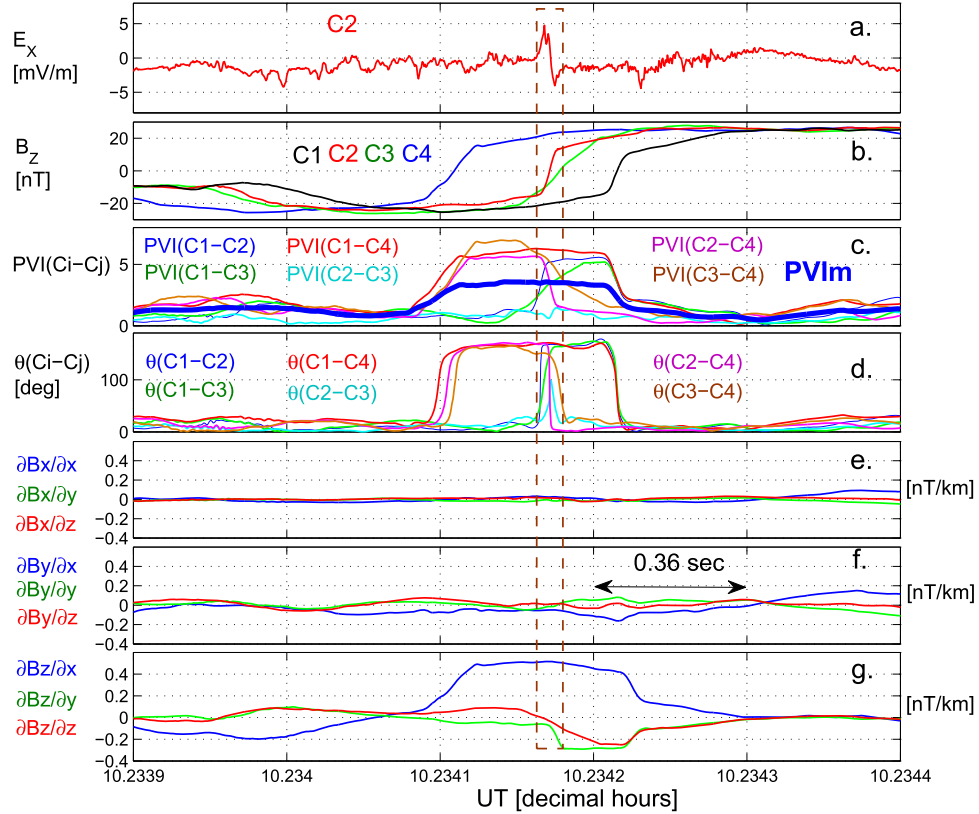


Figure 3. Example of a current sheet. This event and the current associated electron heating have already been studied by Chasapis et al. (2015b). (a) Normal electric field E_x ; (b) B_z components of the magnetic field; (c) partial variances of increments: $\text{PVI}(C_i-C_j, t) \equiv \text{PVI}_{ij}(t)$ and $\text{PVI}_m(t)$; (d) magnetic field rotational angles $\theta(C_i-C_j, t) \equiv \theta_{ij}(t)$; (e)–(g) partial derivatives of magnetic field components.

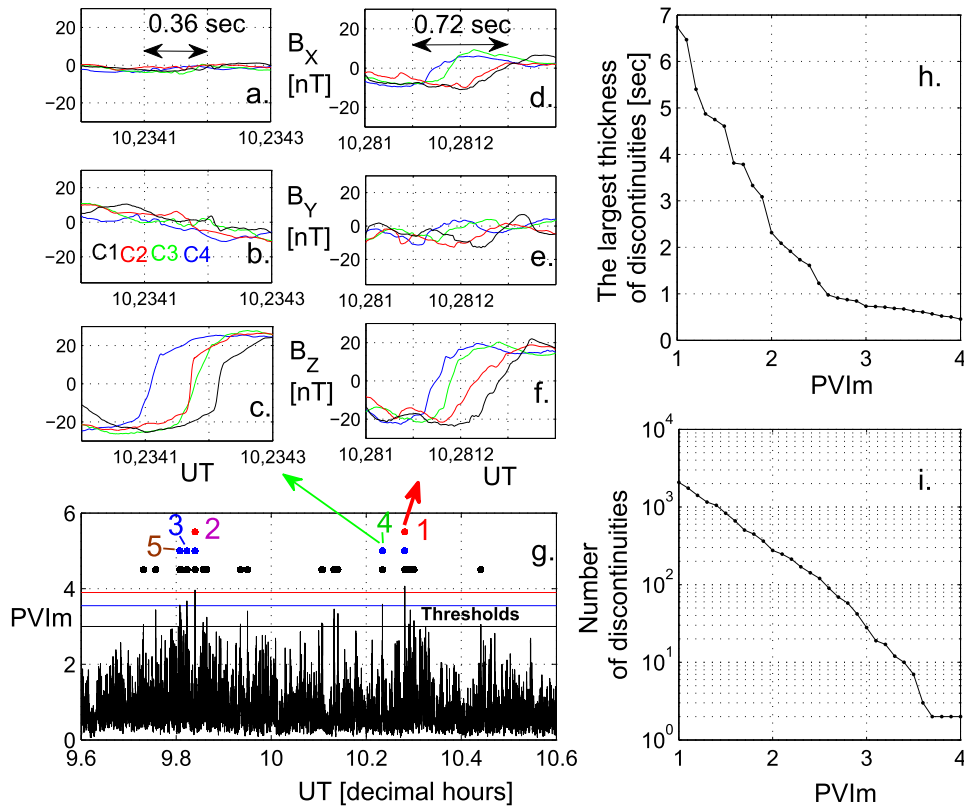


Figure 4. Examples of current sheets with width 0.36 s (panels (a)–(c)) and 0.72 s (panels (d)–(f)); (g) PVI_m magnitude with three levels of threshold (horizontal lines in red, blue, and black) and their respective current sheets (colored dots). The five strongest discontinuities are color coded in red, magenta, blue, green, and brown. The arrows mark the positions of the two selected events (1 and 4) in (a)–(c) (previously studied by Chasapis et al. (2015b)) and (d)–(f) (previously studied by Retinò et al. (2007)); (h) and (i) show the discontinuity thickness and number vs. PVI_m , respectively.

GSE coordinate system was shown to be very close to the current sheet system. The panels show the bipolar change of the electric field E_X (C2) 3(a), the B_Z (C1, C2, C3, C4) components of the magnetic field 3(b), PVI_{*i*} for spacecraft pairs and the mean PVI_m 3(c), θ_s for spacecraft pairs 3(d), and the derivatives ∂_{ij} 3(e)–(g). The bipolar E_X (C2) signature is associated with the fast, ~ 0.06 s long sign change of B_Z (C2) within the dashed box. The average Doppler-shifted electron gyroperiod for the considered 1 hr long interval is ~ 0.04 s, rather close to the duration of the bipolar electric field change. This thin electron current sheet is embedded into a broader sheet associated with the more gradual changes of B_Z before and after of the dashed box. The fastest sign changes of B_Z in Figure 3(b) were observed by C1 and C2, indicating that these probes crossed the current sheet where it was locally thinner or in a direction more perpendicular than the other probes. Since the C1–C2 probes are separated mainly in the Y and Z directions (Figure 1), the current sheet normal direction is close to the GSE X direction. This is also confirmed by minimum variance analysis (not shown). Therefore, the normal component of the electric field is $E_n \sim E_X$ (Figure 3(a)), exhibiting the same timescale as the embedded electron scale seen in B_Z (red curve in the dashed box, Figure 3(b)). Figures 3(c) and (d) show that the PVI_{ij} or PVI_m and θ_{ij} parameters are correlated and indicate the crossings of the thin current sheet rather well. $\theta_{ij} \sim 180^\circ$ implies that the current sheet is between a spacecraft pair while $\theta_{ij} \sim 0^\circ$ indicates that the probes are at the same side of the sheet. The derivatives of the B_Z component mark the presence of the current sheet (Figure 3(g)); the other ∂_{ij} s show only insignificant fluctuations (Figures 3(e)–(f)). Some events

during the analyzed interval are associated with the sign changes and enhanced gradients of the B_Y component.

5. CURRENT SHEET AND DISCONTINUITY STATISTICS

The potential discontinuities in the data can be found using the mean PVI_m . In any case, however, the PVI thresholds should not be considered as unique parameters identifying the thin current sheets. For the selected cases here we considered all the parameters shown in Figure 3 and visually checked the events. The usefulness of PVI_m is demonstrated in Figure 4(g), where three different thresholds (red, blue, and black horizontal lines) and the corresponding time instants—points—are shown. The red, blue, and black populations of points correspond to the PVI_m thresholds of the same color. The first five discontinuities are numbered and color coded by red, magenta, blue, green, and brown. This color code is also used in Figure 5 to indicate the location of discontinuities in a histogram. The first discontinuity (magnetic components are depicted in Figures 4(d)–(f)) is a magnetic reconnection event described thoroughly by Retinò et al. (2007). The second discontinuity is a current sheet with B_Y sign changes, and the third discontinuity is a more complicated event comprising crossings of two neighboring current sheets. The fourth discontinuity (Figures 4(a)–(c)) was identified as a current sheet associated with electron heating by Chasapis et al. (2015b). For these current sheets, the maxima of θ_{ij} are close to 180° . The fifth discontinuity is a current sheet where the maxima of θ_{ij} are less than 120° , which is still a very high magnetic shear angle (Chasapis et al. 2015b).

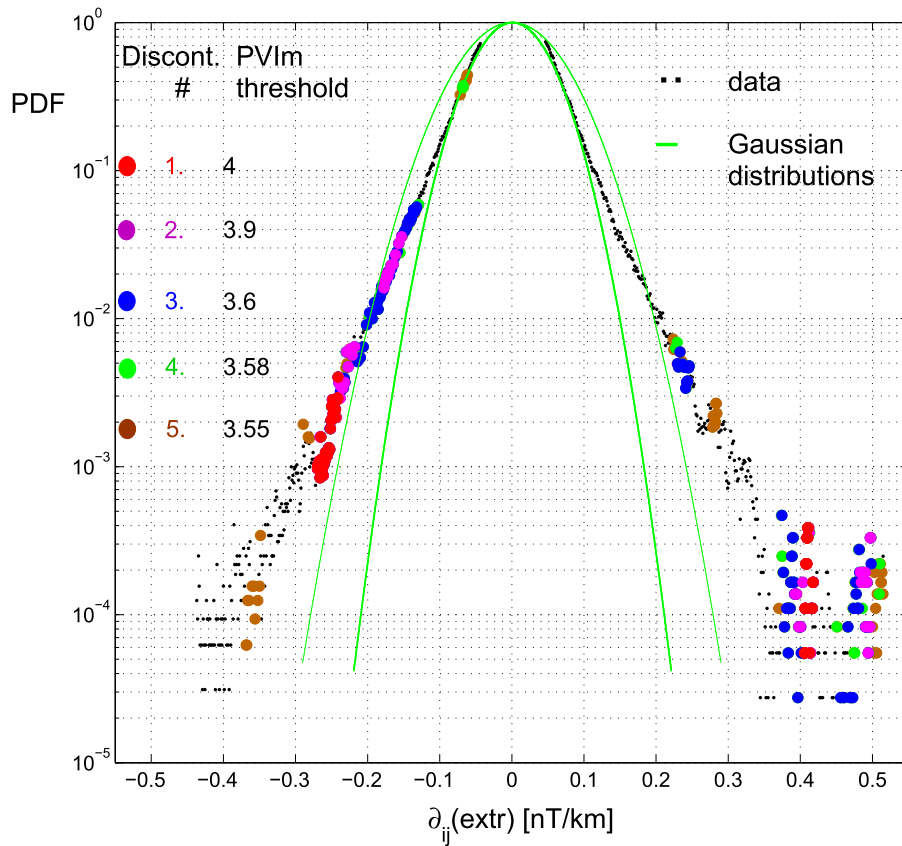


Figure 5. PDF calculated from extremal values of magnetic field partial derivatives. The first five strongest discontinuities from Figure 4(g) are color-coded points at the tail of the PDF. Black points show the data, and green lines correspond to Gaussian distributions.

Figure 4(h) shows the largest thickness of discontinuities in seconds for changing thresholds PVI_m . It is calculated as a local duration of a discontinuity in time, with $PVI_m \geq \text{threshold}$. Since for a given threshold a discontinuity may be represented by one $PVI_m \geq \text{threshold}$ value only, the smallest thicknesses are often close to 0 s. Therefore, the mean discontinuity thickness has no meaning. However, the largest thickness (Figure 4(h)) together with the total number of detected discontinuities (Figure 4(i)) for a given PVI_m threshold provides information about the minimum number of discontinuities with thicknesses equal to or smaller than the largest thickness. The comparison of Figure 4(h) with Figure 4(i) shows that for very thin structures, for example with a duration of less than one second (possibly current sheets), there exist almost one hundred discontinuities during the analyzed magnetosheath interval. Nevertheless, Figure 4(g) demonstrates that the strongest discontinuities represent a tiny part of the time series only. In order to show that the intermittently occurring rare current sheets belong to the tails of PDFs, as is expected from 2D MHD simulations of current density distributions (Greco et al. 2009), the PDF(j) should be obtained directly from the data. Although non-Gaussian skewed distributions are typical for space plasmas (Burlaga & Ness 1998; Vörös et al. 2015), the direct estimation of j from in situ data is difficult. The curlometer technique provides an estimate of $(\nabla \times \mathbf{B})$, but it is loaded by several known sources of errors (Vallat et al. 2005). The curlometer works satisfactorily for well selected, short, and stationary events with a linear variation of B inside the tetrahedron. This is not the case for the entire one-hour interval analyzed here. To

reconstruct the whole PDF(j), the localized strong currents (PDF tail), the nearly current-free flux tube regions, and the random transient currents (central part of the PDF) should all be involved in a histogram. However, the quality of the current density estimation for the considered time interval is low. This can be deduced from the ratio $\text{div } \mathbf{B}/|\nabla \times \mathbf{B}|$, which has values $\gg 1$ for large parts of the data. For good quality (j) estimations, it should be $\ll 1$ (Grimald et al. 2012). This is why instead of the derived quantity $(\nabla \times \mathbf{B})$, which can also be burdened with additional errors, we use the partial derivatives ∂_{ij} for further statistical investigations. However, as Figures 3(e)–(g) show, some of the ∂_{ij} s are close to zero even during current sheet crossing. On the other hand, there exist nonzero ∂_{ij} values which are not associated with the current sheet. The simplest way to obtain PDF(∂_{ij}) is to take the extreme value of $\partial_{ij}(\text{extr}, t) = \max(\partial_{ij}(t))$ or $=\min(\partial_{ij}(t))$ at times t . Physically, we select structures that are associated with the largest magnetic gradient between spacecraft pairs in the tetrahedron volume at times t . The result is shown in Figure 5. The black points correspond to the histogram of the entire time series of $\partial_{ij}(\text{extr}, t)$. The left (negative values) and the right (positive values) of PDF($\partial_{ij}(\text{extr})$) are obtained independently. Since the extreme value distribution has very low occurrence frequencies for small values of derivatives, the central noisy part of the histogram for $-0.05 < \partial_{ij}(\text{extr}) < 0.05$ (nT km⁻¹) is cut off. The color-coded points on the PDF curve, according to their $\partial_{ij}(\text{extr})$, correspond to the five current sheets for different thresholds PVI_m shown in Figure 4(g). We note that the boxes in histograms near a given value of $\partial_{ij}(\text{extr})$ contain contributions from many other time intervals. Nevertheless, for

the purposes of this study, it was enough to show that the strong discontinuities belong to the histogram boxes at the tails of PDFs. The green curves in Figure 5 correspond to Gaussian distributions. The smallest values are normally distributed, while at the non-Gaussian tail the strongest discontinuities are observed, as is expected from numerical simulations (Greco et al. 2009; Servidio et al. 2009; Matthaeus et al. 2015). The wider Gaussian in Figure 5 has the same mean and standard deviation as the data. The narrower Gaussian represents a fit to the central part of the histogram, shown to indicate the strong deviation of the tails from the normal PDF. The PDF values between the two Gaussian curves are expected to correspond to magnetic structures, possibly flux tubes (Greco et al. 2009).

6. SUMMARY AND CONCLUSIONS

The main aim of this study was to show that the thin current sheets identified by simple structure detection tools populate the fat tails of PDFs. This has already been shown for the histograms of the normalized current density in MHD turbulence simulations (Greco et al. 2009; Matthaeus et al. 2015). However, in simulations the identification of current and magnetic structures forming the non-Gaussian PDF (j) is straightforward. Although the four-point curlometer technique is an excellent tool for estimating $j(t)$ from four-spacecraft data, it works well for selected short events only. The two-point magnetic field differences have already been used previously in turbulence studies to obtain the long tail PDFs (Vörös et al. 2006) and to identify the intermittency effects (Yordanova et al. 2015). The extremal values of magnetic field partial derivatives calculated between spacecraft pairs are also associated with thin current sheets. We found that the strongest current sheets associated with $\partial_{ij}(\text{extr})$ belong to the tails of PDF($\partial_{ij}(\text{extr})$), confirming the results of MHD turbulence simulations on the generation of intermittent structures (Greco et al. 2009; Matthaeus et al. 2015). It was also found that over one hour *Cluster* observed about a hundred thin magnetic structures in the MS downstream of a quasi-parallel BS that might be associated with non-homogenous localized heating of plasma. This conjecture has to be confirmed by a thorough analysis of similar events using high-resolution field, particle, and plasma data from the MMS mission. Our results also demonstrate that a conditional selection of structures and their identification in histograms (PDFs) represents a powerful tool for better understanding of the role of rare but intense events (in our case strong discontinuities or reconnection sites), which can determine the basic physical properties of plasma systems.

Z.V. was supported by the Austrian Fond zur Förderung der wissenschaftlichen Forschung (project P24740-N27). The research leading to these results has received funding from the European Community's Seventh Framework Programme ([7/2007–2013]) under grant agreement No. 313038/STORM.

REFERENCES

- Balogh, A., Dunlop, M. W., Cowley, S. W. H., et al. 1997, *SSRv*, **79**, 65
 Burlaga, L. F., & Ness, N. F. 1998, *JGR*, **103**, 29719
 Chang, T., Tam, S. W. Y., & Wu, C. C. 2004, *PhPI*, **11**, 1287
 Chasapis, A. 2015a, PhD thesis, Laboratoire de Physique des Plasmas, Univ. Paris-Sud
 Chasapis, A., Retinò, A., Sahraoui, F., et al. 2015b, *ApJL*, **804**, L1
 Consolini, G., Materassi, M., Marcucci, M. F., & Pallochchia, G. 2015, *ApJ*, **812**, 84
 Cornilleau-Wehrlin, N., Chauveau, P., Louis, S., et al. 1997, *SSRv*, **79**, 107
 Facskó, G., Németh, Z., Erdős, G., Kis, A., & Dandouras, I. 2009, *AnGp*, **27**, 2057
 Farris, M. H., & Russell, C. T. 1994, *JGR*, **99**, 17681
 Greco, A., Chuychai, P., Matthaeus, W. H., Servidio, S., & Dmitruk, P. 2008, *GeoRL*, **35**, L19111
 Greco, A., Matthaeus, W. H., Servidio, S., Chuychai, P., & Dmitruk, P. 2009, *ApJL*, **691**, L111
 Grimald, S., Dandouras, I., Robert, P., & Lucek, E. 2012, *AnGp*, **30**, 1597
 Gustafsson, G., Boström, R., Holback, B., et al. 1997, *SSRv*, **79**, 137
 Hoppe, M. M., Russell, C. T., Frank, L. A., Eastman, T. E., & Greenstadt, E. W. 1981, *JGR*, **86**, 4471
 Karimabadi, H., Roytershteyn, V., Vu, H. X., et al. 2014, *PhPI*, **21**, 062308
 Kovács, P., Facskó, G., & Dandouras, I. 2014, *P&SS*, **92**, 24
 Lucek, E., Horbury, T., Balogh, A., Dandouras, I., & Rème, H. 2004, *AnGp*, **22**, 2309
 Matthaeus, W. H., Wan, M., Servidio, S., et al. 2015, *RSPTA*, **373**, 20140154
 Omid, N., Sibeck, D., Gutynska, O., & Trattner, K. J. 2014, *JGR*, **119**, 2593
 Osman, K. T., Matthaeus, W. H., Gosling, J. T., et al. 2014, *PhRvL*, **112**, 215002
 Osman, K. T., Matthaeus, W. H., Wan, M., & Rappazzo, A. F. 2012, *PhRvL*, **108**, 261102
 Retinò, A., Sundkvist, D., Vaivads, A., et al. 2007, *NatPh*, **3**, 236
 Servidio, S., Greco, A., Matthaeus, W. H., Osman, K. T., & Dmitruk, P. 2011, *JGR*, **116**, A09102
 Servidio, S., Matthaeus, W. H., Shay, M. A., Cassak, P. A., & Dmitruk, P. 2009, *PhRvL*, **102**, 115003-1
 Shue, J.-H., Song, P., Russell, C. T., et al. 1998, *JGR*, **103**, 17791
 Sundkvist, D., Retinò, A., Vaivads, A., & Bale, S. D. 2007, *PhRvL*, **99**, 025004
 Vallat, C., Dandouras, I., Dunlop, M., et al. 2005, *AnGp*, **23**, 1849
 Vörös, Z., Leitner, M., Narita, Y., et al. 2015, *JGR*, **120**, 6152
 Vörös, Z., Baumjohann, W., Nakamura, R., Volwerk, M., & Runov, A. 2006, *SSRv*, **122**, 301
 Yordanova, E., Perri, S., Sorriso-Valvo, L., & Carbone, V. 2015, *EPL*, **110**, 19001
 Yordanova, E., Vaivads, A., André, M., Buchert, S. C., & Vörös, Z. 2008, *PhRvL*, **100**, 205003
 Zhang, L., He, J., Tu, C., et al. 2015, *ApJL*, **804**, L43